


DOI 10.24425/aee.2022.140208

High-performance induction motor drive based on adaptive super-twisting sliding mode control approach

SALAH EDDINE FARHI  , DJAMEL SAKRI , NOUREDDINE GOLÉA 

Laboratory of Electrical Engineering and Automatic, LGEA, Larbi Ben M'hidi University
Oum El Bouaghi, Algeria

e-mail:  salahfarhi04@gmail.com, {sk_djamel/nour_golea}@yahoo.fr

(Received: 28.05.2021, revised: 26.10.2021)

Abstract: This paper proposes two high-order sliding mode algorithms to achieve high-performance control of induction motor drive. In the first approach, the super-twisting algorithm (STA) is used to reduce the chattering effect and to improve control accuracy. The second approach combines the super-twisting algorithm with a quasi-barrier function technique. While the super-twisting algorithm (STA) aims at the chattering reduction, the Barrier super-twisting algorithm (BSTA) aims to eliminate this phenomenon by providing continuous output control signals. The BSTA is designed to prevent the STA gain from being over-estimated by making these gains to decrease and increase according to system's uncertainties. Stability and finite-time convergence are guaranteed using Lyapunov's theory. In addition, the two controlled variables, rotor speed, and rotor flux modulus are estimated based on the second-order sliding mode (SOSM) observer. Finally, simulations are carried out to compare the performance and robustness of two control algorithms without adding the equivalent control. Tests are achieved under external load torque, varying reference speed, and parameter variations.

Key words: barrier function, chattering, gains adaptation, induction motor drive, sliding mode control, super twisting

1. Introduction

The optimal selection of electric motor drives and their control techniques are essential for high-performance achievement in industrial applications. For instance, an induction motor (IM) is one of the machines that convert electrical energy into production systems, it is also used in many applications such as robots, conveyor systems, traction, medical equipment, cranes,



© 2022. The Author(s). This is an open-access article distributed under the terms of the Creative Commons Attribution-NonCommercial-NoDerivatives License (CC BY-NC-ND 4.0, <https://creativecommons.org/licenses/by-nc-nd/4.0/>), which permits use, distribution, and reproduction in any medium, provided that the Article is properly cited, the use is non-commercial, and no modifications or adaptations are made.

wind power and electric vehicles. This wide use is due to IM simple construction, low cost and robustness [1, 2].

Due to its simplicity, PI control is often used in IM drive control loops. However, PI control is generally sensitive to parameters variation and disturbances [3]. Recently, many sliding mode control (SMC) based robust control techniques have been proposed to improve IM drives performance [4]. SMC is a nonlinear control technique that has proven its ability to guarantee robustness and performance [5]. The SMC approach has a simple design and implementation with fast response and ability to deal with complex characteristics, such as nonlinearities, model uncertainties, and it is robust regarding unmodeled perturbations [6, 7]. The principle of SMC is to drive and constrain the system state trajectory to slide along a predefined sliding surface using switching control structure [8]. However, due to finite switching frequency in a neighborhood of the sliding surface, an undesirable high-frequency chattering phenomenon occurs. The chattering phenomenon can be amplified by the existence of fast parasitic dynamics in the systems [9] or by discontinuous control implementation [10, 11] along with control high gain [12]. The chattering can lead to control accuracy degradation, can make the system unstable, or even worse, it might lead to mechanical pieces rupture [12, 13]. The above aspects reduce the applicability of SMC in some domains such as electric drives control and position control.

In order to significantly reduce chattering and achieve optimum control effect, several composite sliding mode controls were introduced as in [14], where a hybrid reaching law was used, and it was verified that the new law yields smaller chattering and offers a better dynamic response. Further, in [15] a hybrid wolf optimization algorithm was proposed to automatically adjust a sliding mode direct torque control the control parameters. The above technique showed rapid convergence and low torque ripples for PMSM drive.

Some researchers have been interested in using higher-order sliding mode algorithms to reduce chattering effects. The super-twisting algorithm (STA), an extension of a high-order sliding mode (HOSM), has created strong interest and has got one of the most control techniques cited in the last two decades. The STA approach produces a continuous control action and ensures trajectory convergence for systems with relative degree one [16, 17]. STA control application to IM drives exhibits simplicity of design, reduction of the chattering problem and low-cost implementation [18, 19]. However, in practice, the STA control is not able to completely remove the chattering effect, as low-magnitude fast-oscillations are still produced in the vicinity of the sliding surface [16]. Fast-oscillations are due to the algorithm switching gains, because in most cases these gains are designed relatively large to guarantee the system stability, which consequently lead to high frequency activity.

In order to eliminate chattering, resulting from over-estimated switching gains, several improvements have been proposed. In [16], STA gains are provided through describing the function method to adjust the fast-oscillations produced in systems with fast-actuators. In [20], STA gains are adjusted to minimum acceptable values to reduce the chattering effect, along with maintaining a finite-time convergence. Further in [21], a variable gain STA is proposed to alleviate the chattering effect together with compensation of bounded uncertainties. The first idea was to adapt the STA gains by increasing them until the sliding mode is detected, and then fixing them at these values [22]. However, this technique can lead to over-estimated switching gains since uncertainty/perturbation are not fixed. A solution was to adapt these gains to increase and decrease according to the effect of disturbances on the system. Recently, the barrier function has been

proposed to guarantee that SMC switching gains are not over-estimated, along with minimizing the effects of chattering and ensuring sliding surface convergence [22–25].

Regarding the STA control applied to IM drives, there is some research in the literature. In [26], PI control was replaced by the STA to control the IM speed and flux. Further, an STA-based observer was added to estimate required variables. The algorithm was tested against variations in IM resistances values. The result was satisfactory in steady-state, but the STA control was designed with an equivalent control term, which increases the computing burden. As an effort to improve the control performance, in [27], the equivalent control term has been dispensed and the IM was controlled by combining feedback linearization and the STA. The result was a robust closed-loop system. In [27, 28] an equivalent control term was perceived as a disturbance to the system and compensated by adjusting the gains according to the actual perturbations boundaries, which also leads to an over-estimation of switching control gains when the disturbance takes a small value. On the other hand, works in [17, 29] describe the STA control with conventional direct torque control (DTC), applied to the IM drive. It is shown that the exponent parameter in an STA nonlinear term has a significant effect on steady-state and transient performances. In addition, the conclusion was that exponent parameter values between 0.1 and 0.5 should minimize chattering and provide a fast response for low power drives.

The control design is dependent on state variable feedback rotor speed and rotor flux measurements which are not easily available, especially since flux sensors are usually not available and speed sensors are expensive. For these reasons, several methods based on sliding mode have been developed for estimating IM variables. Among the observation techniques used, we can cite the SOSM observers [30, 31], composite sliding mode disturbance observer (SMDO) [32].

Inspired by [25], this paper proposes the combination of the STA and barrier function technique. The resulting BSTA approach updates control gains with respect to system disturbance magnitude. This approach provides means to avoid control over-estimation of the gains and to reduce the chattering effect. The proposed BSTA is applied to the IM drive control. To further point out BSTA performance, a comparison is made with the standard STA control. The simulation results illustrate significant amelioration in the transient and steady-state performance.

The rest of the paper is organized as follows. Section 2 presents the mathematical model of the IM in the stationary reference frame. Section 3 details the SOSM control design along with its stability analysis. Rotor flux and speed estimation, based on the SOSM observer, is developed in section 4. In section 5, simulation tests and results are presented and discussed. Some concluding remarks are pointed out in section 6.

2. IM modeling

The mathematical model of a three-phase induction motor, in a fixed reference frame, is given by:

$$\begin{aligned}
 \dot{i}_{\alpha s} &= -\gamma i_{\alpha s} + a_1 b_1 \phi_{\alpha r} + b_1 \omega \phi_{\beta r} + \frac{1}{\sigma} v_{\alpha s}, & \dot{i}_{\beta s} &= -\gamma i_{\beta s} + a_1 b_1 \phi_{\beta r} - b_1 \omega \phi_{\alpha r} + \frac{1}{\sigma} v_{\beta s}, \\
 \dot{\phi}_{\alpha r} &= -a_1 \phi_{\alpha r} - \omega \phi_{\beta r} + a_1 M i_{\alpha s}, & \dot{\phi}_{\beta r} &= -a_1 \phi_{\beta r} + \omega \phi_{\alpha r} + a_1 M i_{\beta s}, \\
 \dot{\Omega} &= \mu (\phi_{\alpha r} i_{\beta s} - \phi_{\beta r} i_{\alpha s}) - \frac{T_L}{J},
 \end{aligned} \tag{1}$$

where: $i_{\alpha,\beta s}$, $v_{\alpha,\beta s}$, $\phi_{\alpha,\beta r}$ are the stator currents, stator voltages and rotor flux components; ω is the electrical angular speed; J is the inertia moment and T_L is the load torque; a_1 , b_1 , σ , μ , γ are the positive constants given by:

$$\sigma = L_s \left(1 - M^2 / (L_s L_r) \right), \quad b_1 = M / (\sigma L_r), \quad a_1 = R_r / L_r,$$

$$\gamma = R_s / \sigma + a_1 b_1 M, \quad \mu = p M / (J L_r),$$

where: $R_s R_r$ are the stator and rotor resistances; $L_s L_r M$ are the stator, rotor and mutual inductances.

3. HOSM Control

A HOSM control will be designed to operate the IM in a high-performance application, while reduce the chattering. Here, the speed error $e_1 = \Omega^* - \Omega$ and flux magnitude error $e_2 = \phi_r^{*2} - \phi_r^2$ are chosen as controlled variables, where $\phi_r^2 = \phi_{\alpha r}^2 + \phi_{\beta r}^2$ and $\Omega^* \phi_r^*$ are desired reference trajectories for rotor speed and flux magnitude.

The switching functions are chosen as:

$$s_1 = c_1 e_1 + \dot{e}_1, \quad (2)$$

$$s_2 = c_2 e_2 + \dot{e}_2,$$

where: c_1 , c_2 represent the positive constant to be chosen according to the control performance objective.

The control objective is to force rotor speed and flux magnitude to track desired references. First, let's find the derivatives of sliding surfaces:

$$\dot{s}_1 = c_1 \dot{e}_1 + \ddot{e}_1, \quad (3)$$

$$\dot{s}_2 = c_2 \dot{e}_2 + \ddot{e}_2.$$

Eq. (3) can be rewritten in a matrix form as:

$$\begin{bmatrix} \dot{s}_1 \\ \dot{s}_2 \end{bmatrix} = \begin{bmatrix} f_1 \\ f_2 \end{bmatrix} - AB \begin{bmatrix} v_{\alpha s} \\ v_{\beta s} \end{bmatrix}, \quad (4)$$

where:

$$A = \begin{bmatrix} \frac{\mu}{\sigma} & 0 \\ 0 & \frac{2a_1 M}{\sigma} \end{bmatrix}, \quad B = \begin{bmatrix} -\phi_{\beta r} & \phi_{\alpha r} \\ \phi_{\alpha r} & \phi_{\beta r} \end{bmatrix}. \quad (5)$$

The stator voltage $v_{\alpha s}$, $v_{\beta s}$ are the control inputs and $f_{1,2}$ is defined as follows:

$$f_1 = -\mu (a_1 + \gamma - c_1) (\phi_{\beta r} i_{\alpha s} - \phi_{\alpha r} i_{\beta s}) + \mu \omega b_1 \phi_r^2 + \mu \omega (\phi_{\alpha r} i_{\alpha s} + \phi_{\beta r} i_{\beta s}) +$$

$$+ c_1 \left(\frac{T_L}{J} + \dot{\Omega}^* \right) + \frac{\dot{T}_L}{J} + \ddot{\Omega}^*, \quad (6)$$

$$f_2 = -2a_1 (2a_1 - c_2 + a_1 b_1 M) \phi_r^2 + 2a_1 M (3a_1 + \gamma - c_2) (\phi_{\alpha r} i_{\alpha s} + \phi_{\beta r} i_{\beta s}) -$$

$$- 2a_1^2 M^2 (i_{\alpha s}^2 + i_{\beta s}^2) + 2a_1 M \omega (\phi_{\beta r} i_{\alpha s} - \phi_{\alpha r} i_{\beta s}) + c_2 \dot{\phi}_r^* + \ddot{\phi}_r^*.$$

3.1. Super twisting algorithm controller

The use of the super-twisting algorithm allows overcoming any perturbations with bounded derivatives. In addition, when applying this algorithm, it does not need any information about the sliding surface derivative. The STA control is introduced as follows:

$$\begin{bmatrix} v_{\alpha s}^{st} \\ v_{\beta s}^{st} \end{bmatrix} = \begin{bmatrix} \lambda_{11}|s_1|^{1/2}\text{sign}(s_1) + \lambda_{12} \int \text{sign}(s_1) dt \\ \lambda_{21}|s_2|^{1/2}\text{sign}(s_2) + \lambda_{22} \int \text{sign}(s_2) dt \end{bmatrix}. \quad (7)$$

The STA, without equivalent control term, is given by:

$$\begin{bmatrix} v_{\alpha s} \\ v_{\beta s} \end{bmatrix} = B^{-1} \begin{bmatrix} v_{\alpha s}^{st} \\ v_{\beta s}^{st} \end{bmatrix} = B^{-1} \begin{bmatrix} \lambda_{11}|s_1|^{1/2}\text{sign}(s_1) + \lambda_{12} \int \text{sign}(s_1) dt \\ \lambda_{21}|s_2|^{1/2}\text{sign}(s_2) + \lambda_{22} \int \text{sign}(s_2) dt \end{bmatrix}, \quad (8)$$

where: λ_{11} , λ_{12} , λ_{21} , λ_{22} are the positive gains, to be designed to ensure system stability. From STA control law (8), the sliding surface dynamic (4) becomes:

$$\begin{bmatrix} \dot{s}_1 \\ \dot{s}_2 \end{bmatrix} = \begin{bmatrix} f_1 \\ f_2 \end{bmatrix} - A \begin{bmatrix} \lambda_{11}|s_1|^{1/2}\text{sign}(s_1) + \lambda_{12} \int \text{sign}(s_1) dt \\ \lambda_{21}|s_2|^{1/2}\text{sign}(s_2) + \lambda_{22} \int \text{sign}(s_2) dt \end{bmatrix}, \quad (9)$$

where: $f_{1,2}$ is assumed to represent the terms of bounded perturbations. The stability proof of the STA and the states convergence can be found in [27, 34].

3.2. Barrier function based super twisting algorithm

Barrier functions have been used in many adaptation techniques, such as in [35] to guarantee that the constraints are not transgressed for nonlinear systems outputs and in [36] to adapt the gains of Levant's differentiator. The idea of barrier functions is that when its arguments approach some predefined restrictions, the output tends to infinity (see Fig. 1 left). Recently and thanks to its features, the barrier function is also applied to a certain class of SMC, as in [23] this strategy has been suggested for a first-order SMC, and in [24] it has been proposed to adapt the twisting control gains.

In [25], the barrier function has been modified to the quasi-barrier function QBF (see Fig. 1 right). The idea of QBF technique is to enforce the STA gains to decrease and increase with respect to the sliding functions in a certain region, and maintains these gains constant outside this region.

The barrier function, a continuous positive-semi definite function on the interval $x \in]-\varepsilon, \varepsilon[$, is given by:

$$K_{BF}(x) = \tilde{L} \frac{|x|}{\varepsilon - |x|}, \quad \varepsilon > 0. \quad (10)$$

This function is strictly increasing on $x \in [0, \varepsilon[$ and has a unique minimum at zero:

$$K_{BF}(x) \in [b, +\infty[\quad \lim_{|x| \rightarrow \varepsilon} K_{BF}(x) = +\infty, \quad K_{BF}(0) = b, \quad b \geq 0. \quad (11)$$

The QBF, used to attenuate the chattering, is given by [25]:

$$\tilde{K}_{BF}(x) = \tilde{L} \frac{\text{sat}_{\tilde{\varepsilon}}(|s|)}{\varepsilon - \text{sat}_{\tilde{\varepsilon}}(|s|)}, \quad \tilde{\varepsilon} > 0 \quad \lim_{|x| \rightarrow \varepsilon} \tilde{K}_{BF}(x) = 1, \quad \tilde{K}_{BF}(0) = b, \quad b \geq 0, \quad (12)$$

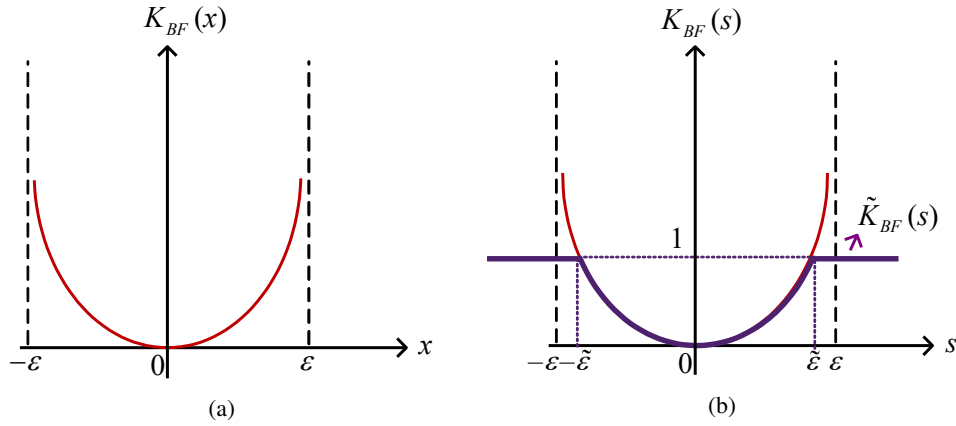


Fig. 1. Barrier function techniques: barrier function (a); quasi barrier function (b)

where: \tilde{L} , ε , $\tilde{\varepsilon}$ are the positive constants and the saturation function is defined as:

$$\text{sat}_{\tilde{\varepsilon}}(s) = \begin{cases} s & \text{for } |s| < \tilde{\varepsilon} \\ \tilde{\varepsilon} \text{ sign}(s) & \text{for } |s| \geq \tilde{\varepsilon} \end{cases} \quad (13)$$

The QBF takes low value when $|s| < \tilde{\varepsilon}$, and the STA gains adapt, which will decrease accordingly. Alternatively, the QBF takes its highest value (equal to 1) when a disturbance occurs $|s| > \tilde{\varepsilon}$.

For a smooth transition from the STA to the BSTA [25], a barrier function gain, according to (12), (13) and Fig. 1, is set to:

$$\tilde{L}_i = \frac{\varepsilon_i - \tilde{\varepsilon}_i}{\tilde{\varepsilon}_i}, \quad i = 1, 2. \quad (14)$$

The adaptive BSTA control is given by:

$$\begin{bmatrix} v_{\alpha s}^{bst} \\ v_{\beta s}^{bst} \end{bmatrix} = \begin{bmatrix} \tilde{K}_{BF1}(s_1) \left(\lambda_{11}|s_1|^{1/2} \text{sign}(s_1) + \lambda_{12} \tilde{K}_{BF1}(s_1) \int \text{sign}(s_1) dt \right) \\ \tilde{K}_{BF2}(s_2) \left(\lambda_{21}|s_2|^{1/2} \text{sign}(s_2) + \lambda_{22} \tilde{K}_{BF2}(s_2) \int \text{sign}(s_2) dt \right) \end{bmatrix}, \quad (15)$$

where:

$$\tilde{K}_{BFi}(x) = \tilde{L}_i \frac{\text{sat}_{\tilde{\varepsilon}_i}(|s_i|)}{\varepsilon_i - \text{sat}_{\tilde{\varepsilon}_i}(|s_i|)}, \quad i = 1, 2. \quad (16)$$

By replacing (15) with (8), the IM control inputs become:

$$\begin{bmatrix} v_{\alpha s} \\ v_{\beta s} \end{bmatrix} = B^{-1} \begin{bmatrix} v_{\alpha s}^{bst} \\ v_{\beta s}^{bst} \end{bmatrix} = B^{-1} \begin{bmatrix} \tilde{K}_{BF1}(s_1) \left(\lambda_{11}|s_1|^{1/2} \text{sign}(s_1) + \lambda_{12} \tilde{K}_{BF1}(s_1) \int \text{sign}(s_1) dt \right) \\ \tilde{K}_{BF2}(s_2) \left(\lambda_{21}|s_2|^{1/2} \text{sign}(s_2) + \lambda_{22} \tilde{K}_{BF2}(s_2) \int \text{sign}(s_2) dt \right) \end{bmatrix}. \quad (17)$$

3.3. Stability proof of BSTA

By introducing the control inputs (17) in the dynamic of sliding surfaces (4), the closed loop dynamic system becomes:

$$\dot{s}_i = f_i - k_{i1}\tilde{K}_{BFi}(s_i)|s_i|^{1/2} \text{sign}(s_i) + u_i, \quad \dot{u}_i = -k_{i2}\tilde{K}_{BFi}^2(s_i) \text{sign}(s_i), \quad i = 1, 2, \quad (18)$$

where:

$$\begin{bmatrix} k_{11} \\ k_{21} \end{bmatrix} = A \begin{bmatrix} \lambda_{11} \\ \lambda_{21} \end{bmatrix}, \quad \begin{bmatrix} k_{12} \\ k_{22} \end{bmatrix} = A \begin{bmatrix} \lambda_{12} \\ \lambda_{22} \end{bmatrix}. \quad (19)$$

In the next analysis, we assume that $\tilde{K}_{BF}(s) = K_{BF}(s)$. The Lyapunov barrier function is given by [25]:

$$V_{BF}(s_i) = |s_i| + k_{i2}\varepsilon_i^{-1}\tilde{L}_i\tilde{K}_{BFi}(s_i) + \frac{1}{2}u_i^2, \quad i = 1, 2. \quad (20)$$

The time derivative of the Lyapunov barrier function along the trajectories of (18) is given by:

$$\begin{aligned} \dot{V}_{BF}(s_i) &= \frac{s_i}{|s_i|}\dot{s}_i + k_{i2}\tilde{L}_i^2 \frac{\text{sign}(s_i)}{(\varepsilon_i - |s_i|)^2}\dot{s}_i + u_i\dot{u}_i = \\ &= \frac{s_i}{|s_i|} \left(f_i - k_{i1}\tilde{K}_{BFi}(s_i)|s_i|^{1/2} \text{sign}(s_i) + u_i \right) + u_i \left(-k_{i2}\tilde{K}_{BFi}^2(s_i) \text{sign}(s_i) \right) + \\ &\quad + k_{i2}\tilde{L}_i^2 \frac{\text{sign}(s_i)}{(\varepsilon_i - |s_i|)^2} \left(f_i - k_{i1}\tilde{K}_{BFi}(s_i)|s_i|^{1/2} \text{sign}(s_i) + u_i \right). \end{aligned} \quad (21)$$

By introducing (16) into (21) and taking the restrictions $u_i \text{sign}(s_i) \leq |u_i|$, $f_i \text{sign}(s_i) \leq \delta_i$, the time derivative of (21) becomes:

$$\begin{aligned} \dot{V}_{BF}(s_i) &\leq -\frac{k_{i1}\tilde{L}_i}{(\varepsilon_i - |s_i|)^2}|s_i|^{3/2} - \frac{k_{i1}k_{i2}\tilde{L}_i^3}{(\varepsilon_i - |s_i|)^3}|s_i|^{3/2} - \frac{k_{i2}\tilde{L}_i^2}{(\varepsilon_i - |s_i|)^2}|s_i|^2|u_i| \\ &\quad + \left(1 + \frac{k_{i2}\tilde{L}_i^2}{(\varepsilon_i - |s_i|)^2} \right) (|u_i| + \delta_i). \end{aligned} \quad (22)$$

By defining:

$$\Delta = \left(1 + \frac{k_{i2}\tilde{L}_i^2}{(\varepsilon_i - |s_i|)^2} \right) (|u_i| + \delta_i) \Delta > 0. \quad (23)$$

From (22) and (23), one gets:

$$\begin{aligned} \dot{V}_{BF}(s_i) &\leq -\frac{k_{i1}\tilde{L}_i}{(\varepsilon_i - |s_i|)^2}|s_i|^{3/2} - \frac{k_{i1}k_{i2}\tilde{L}_i^3}{(\varepsilon_i - |s_i|)^3}|s_i|^{3/2} - \frac{k_{i2}\tilde{L}_i^2}{(\varepsilon_i - |s_i|)^2}|s_i|^2|u_i| + \Delta \leq \\ &\leq -\frac{k_{i1}k_{i2}\tilde{L}_i^3}{(\varepsilon_i - |s_i|)^3}|s_i|^{3/2} - \frac{k_{i2}\tilde{L}_i^2}{(\varepsilon_i - |s_i|)^2}|s_i|^2|u_i| - \frac{1}{(\varepsilon_i - |s_i|)} \left(k_{i1}\tilde{L}_i|s_i|^{3/2} - (\varepsilon_i - |s_i|)\Delta \right) \leq \\ &\leq -\frac{k_{i1}k_{i2}\tilde{L}_i^3}{(\varepsilon_i - |s_i|)^3}|s_i|^{3/2} - \frac{k_{i2}\tilde{L}_i^2}{(\varepsilon_i - |s_i|)^2}|s_i|^2|u_i| - \frac{\Delta}{(\varepsilon_i - |s_i|)} \left(\frac{k_{i1}\tilde{L}_i|s_i|^{3/2}}{\Delta} + |s_i| - \varepsilon_i \right). \end{aligned} \quad (24)$$

The upper bound of $\dot{V}_{BF}(s_i)$ is given by:

$$\begin{aligned} \dot{V}_{BF}(s_i) \leq & -\frac{k_{i1}k_{i2}\tilde{L}_i^3}{(\varepsilon_i - |s_i|)^3}|s_i|^{3/2} - \frac{k_{i2}\tilde{L}_i^2}{(\varepsilon_i - |s_i|)^2}|s_i|^2|u_i| - \\ & - \frac{\Delta}{(\varepsilon_i - |s_i|)}F_i, \quad i = 1, 2, \end{aligned} \quad (25)$$

where:

$$F_i = \left(\frac{k_{i1}\tilde{L}_i|s_i|^{3/2}}{\Delta} + |s_i| - \varepsilon_i \right), \quad i = 1, 2. \quad (26)$$

Note that asymptotic stability is guaranteed if $\dot{V}_i < 0$, according to (25) the time derivative of the Lyapunov barrier function is negative definite if F_i is positive semi-definite. From (23) and (26) the condition is satisfied if $|s_i| < \varepsilon_i$.

4. SOSM observer

The correct operation and reliability of the IM depend on the fault-free operation of the speed sensor [37]. Consequently, the optimum manner to reduce the space, cost and to improve the performance of the control is to eliminate the sensors and replace them with observers. The observers are selected for any control depending on their performance such as not being affected by disturbances and being able to improve dynamic characteristics, as well as immunity from the noise commonly present in measurements. A higher-order sliding mode observer is suitable for the application because it includes robustness against parameter changes [38], good dynamic characteristics, and at the same time alleviates the chattering behavior.

In our control, the measurements of the rotor speed and rotor flux linkages are needed, but to avoid the above sensor problem, we need to estimate these values. To reach this objective, we will depend on a robust observer that was designed in [31], where it is based on super twisting algorithms. This observer needs simple measurements of the stator current and voltages.

The observer is proposed by the following equations [31]:

$$\begin{aligned} \hat{\phi}_{\alpha r} &= -a_1\hat{\phi}_{\alpha r} - \hat{\omega}\hat{\phi}_{\beta r} + a_1Mi_{\alpha s} + f_{\phi_{\alpha r}}, \\ \hat{\phi}_{\beta r} &= -a_1\hat{\phi}_{\beta r} + \hat{\omega}\hat{\phi}_{\alpha r} + a_1Mi_{\beta s} + f_{\phi_{\beta r}}, \\ \hat{\Omega} &= \mu(\hat{\phi}_{\alpha r}i_{\beta s} - \hat{\phi}_{\beta r}i_{\alpha s}) - \frac{T_L}{J} + f_{\Omega}, \end{aligned} \quad (27)$$

where: $\hat{\phi}_{\alpha, \beta r}$, $\hat{\Omega}$ are the estimates of the rotor fluxes and the rotor speed, respectively, $f_{\phi_{\alpha, \beta r}}$, f_{Ω} are the additional inputs, which have to be designed to guarantee the stability of this observer. In this observer, the STA is used to make the observation error, since the stator currents tend to zero in finite time, more detail about this observer and its stability can be found in [31].

The control loop of the induction motor by the BSTA is shown in Figure 2.

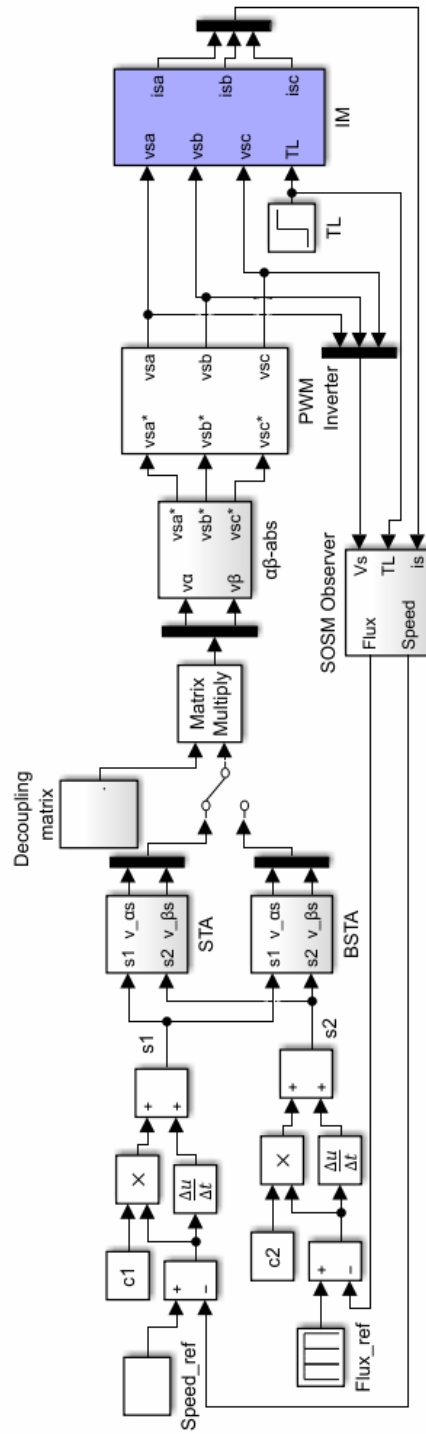


Fig. 2. Block diagram of the BSTA controller

5. Simulation

The computer simulations are created in this section to show the effectiveness of the designed control algorithms by using MATLAB-Simulink software. The IM and designed control algorithms parameters are shown in Table 1. Table 4 contains values of the STA gains. The following figures (Fig. 3) show the comparison between STA efficiency and BSTA adaptation.

Table 1. Parameters of IM [33] and controllers

Parameter name	Symbol	Value	Unit
Nominal power	P_n	1500	W
Stator and rotor inductance	L_s, L_r	0.247	H
Mutual inductance	M	0.258	H
Stator and rotor resistance	R_s, R_r	4.85, 3.805	Ω
Inertia moment	J	0.031	$\text{Kg}\cdot\text{m}^2$
Number of pole pairs	p	2	–
Positive constant for sliding surface	c_1, c_2	300, 230	–
Gain values of STA	$\lambda_{11}, \lambda_{12}, \lambda_{21}, \lambda_{22}$	7600, 250, 8600, 500	–
Positive constants for QFB	$\varepsilon_1, \tilde{\varepsilon}_1$	18, 13	–
Positive constants for QFB	$\varepsilon_2, \tilde{\varepsilon}_2$	3, 1.6	–

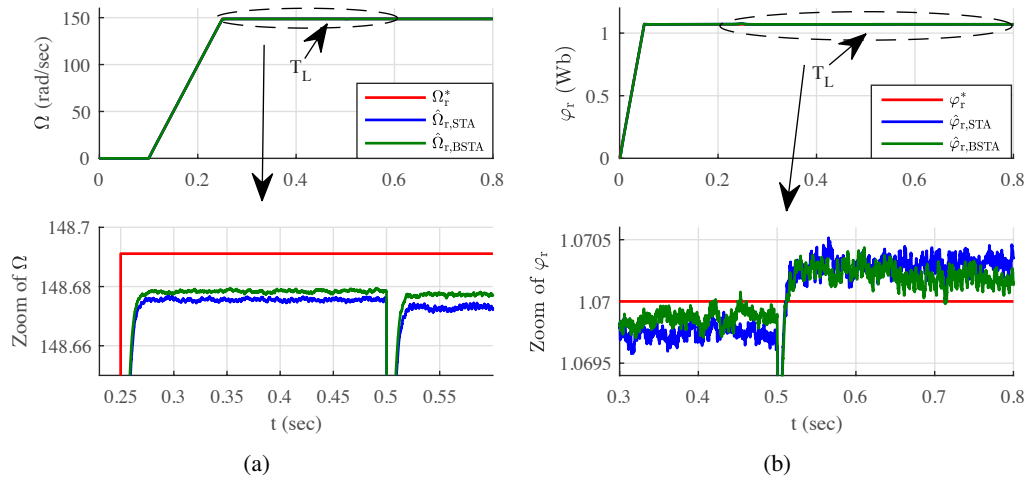


Fig. 3. Results of speed and rotor flux estimation with STA and BSTA: speed tracking performance (a); estimated rotor flux (b)

Figure 3(a) shows the speed estimate response with the STA and BSTA, in both controls, the estimated speed follows the nominal reference (148.69 rad/s) very well and rejects the nominal external load ($T_L = 10$ Nm) at $t = 0.5$ s in a good way. One can notice some steady state errors in both responses (about 0.01 rad/s), this is due to disturbances in the system and the absence of equivalent control in the control loop. The steady state errors can be compensated by increasing the constant value c_1 , but this negatively affects the control, as it leads to significant chattering and overshoot in speed response.

Nevertheless, the graphs show that the BSTA is more precise than the STA, as well the settling time and rise time in the BSTA is somewhat better than in STA, as shown in Table 2. Furthermore, the comparison in terms of THD is given in Table 3, here it was shown that the THD is reduced in BSTA to 2.87% compared to STA where it was 2.99%.

Table 2. Performance comparison for varying reference speed

Reference speed [rad/s]	Controller	Rise time [ms]	Settling time [ms]	Overshoot [%]
0 to 148.69	STA	120.49	142.37	0
	BSTA	120.47	142.35	0

Table 3. Steady-state control performance

Time [s]	Controller	Steady state errors [rad/s]	THD for current [%]
0.6 to 0.7	STA	0.0161	2.99
	BSTA	0.0111	2.87

In Fig. 3(b), the square modulus of rotor flux is illustrated, the reference flux is set at $1.07W_b$. As we can notice, both algorithms have the same flux behavior with identical amplitudes. At time $t = 0.5$ s when the rated load torque is applied, we can see that a small attenuation in rotor flux magnitude square and then disappears thereafter. Zoom illustrates these facts and shows the accuracy of the SOSM observers.

Figure 4(a) presents the stator current response for both algorithms in real axis, it can be seen that there are a few oscillations during the transient regime for both controls around 0.15 s. In steady-state, both currents stabilize at the no-load current about 3.5 A. Due to load torque variation at $t = 0.5$ s, there is a demand for currents, so their value increases to reach approx. 5 A. The response of current by STA or by BSTA is good and with no chattering.

Alternatively, in Fig. 4(b), when the motor torque is shown, there are some oscillations during the tracking of load torque. One can see that the chattering in STA is more than in BSTA. Nevertheless, for two algorithms, the motor torque has a peak at $t = 0.5$ s when applied the load torque and then the motor compensates this load.

Note that Fig. 5(a) illustrates the sliding surfaces under the adaptation of BSTA gains. It can be seen that for both algorithms the sliding mode occurs and the surfaces outputs belong to some neighborhood of zero after the transition regime.

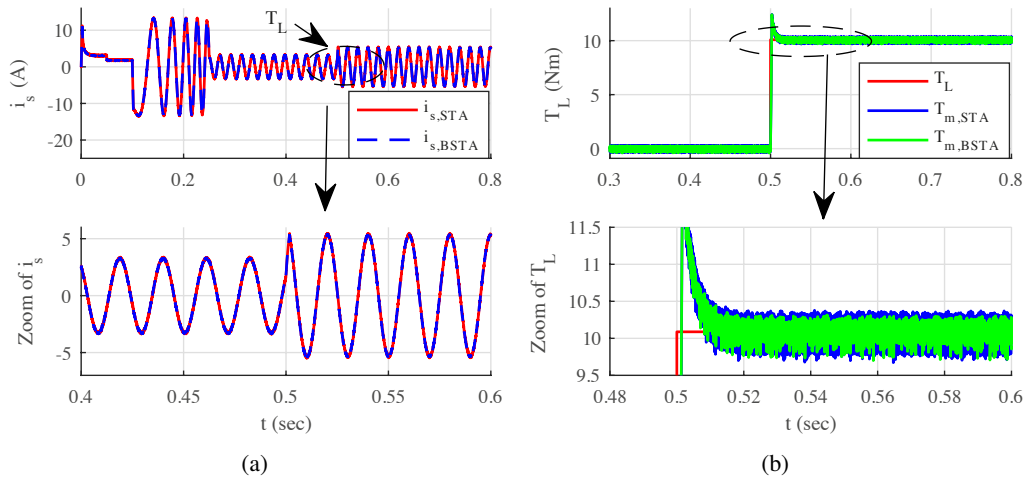


Fig. 4. Results of current and torque for STA and BSTA: current (a); torque (b)

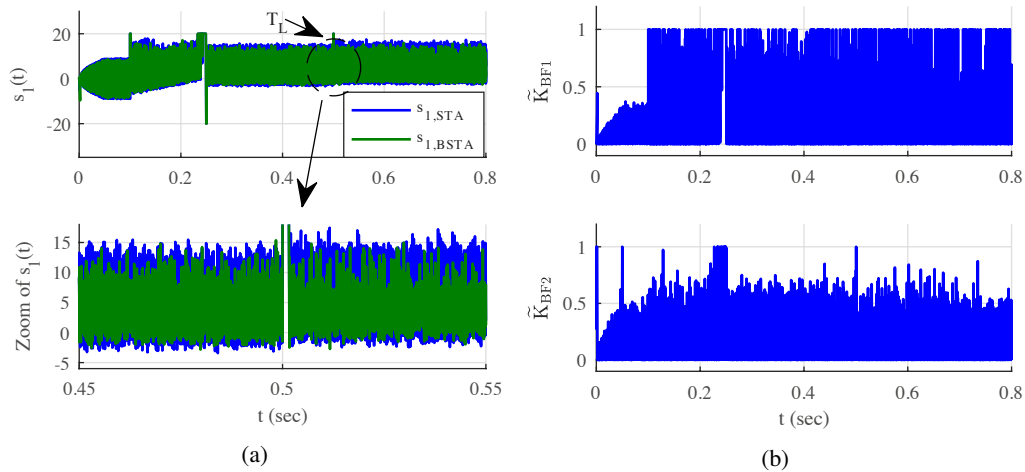


Fig. 5. Sliding surfaces outputs and BSTA gains: surfacesfor speed (a); outputs of BSTA gains (b)

However, these sliding outputs suffer from many oscillations. For both surfaces 1 and 2, this chattering is lower in the BSTA control compared to the STA, because the BSTA control gains are adapted to handle the perturbation without overestimating their values, which delivers more design flexibility with minimizing the amplitude of chattering.

In order to show the performance of the BSTA, the gains of the STA are fixed and shown in Table 4. Figure 5(b) presents the quasi barrier function outputs, these outputs adjust the amplitude of BSTA gains, if this output equals 1 the BSTA gains are the same as the STA gains. Alternatively, if QBF outputs are between 0 and 1, they minimize the BSTA gains values.

Table 4. Some comparison between STA and BSTA gain values

Time [s]	controller	λ_{11}	λ_{12}	λ_{21}	λ_{22}
All time	STA	7600	250	8600	500
0.05	BSTA	661	22.5	8600	500
0.2	BSTA	1140	5.6	86	0.05
0.5	BSTA	7600	250	8600	500
0.7	BSTA	1064	4.9	1720	20

This adaptation can be seen from Table 4, where some BSTA gains' values are displayed during the operation, all these gains remain constant at maximum values during the transit time for compensating the system uncertainties. Then, these gains take several values.

5.1. Speed variation

In this subsection of simulation, the performances of our algorithms have been validated under rated load torque and various speed profiles:

Figure 6(a) shows the speeds tracking performance of the STA and BSTA, the used reference values are: 0, 148.69 and 148.69 rad/s. In this response for both algorithms, we have good tracking performance for estimated speed with their reference values even in low regimes. In the load torque step at 0.8 s, the speed shows a small attenuation that then disappears thereafter to follow their reference values. The performance results are summarized in Table 5, this is shown in the reflection of the reference speed from rad/s to -148.69 rad/s, the rise time of the STA controller is calculated as 120.1 ms, and the settling time is 142.54 ms, these values are reduced

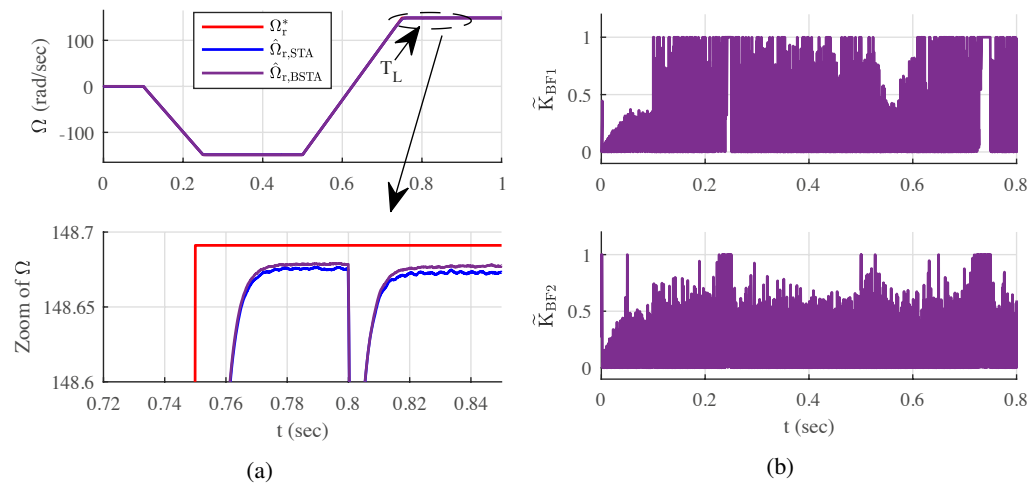


Fig. 6. Results of rotor speed and quasi-barrier function gains under speed variations: speed tracking performance (a); gains versus time (b)

in the BSTA controller, the rise time is calculated as 120 ms, and the settling time is 142.53 ms. In addition, the two algorithms track all reference speed commands without overshoot. These results showed that the BSTA is superior to the STA.

Table 5. Performance comparison for speed reversal operation

Reference speed [rad/sec]	Controller	Rise time [ms]	Settling time [ms]	Overshoot [%]
0 to 148.69	STA	120.1	142.54	0
	BSTA	120	142.53	0

In the same Fig. 6(b), the quasi-barrier function outputs are shown, it can be seen that the gains of the BSTA take maximum values in every change of speed in order to compensate the equivalent control negligent in the control loop.

The sliding surfaces in the STA and BSTA controllers are shown in Fig. 7, it is noted that the system uncertainty is high at the moment when the speed changes, this uncertainty is relatively greater for surface 1. However, at a steady state, the sliding mode occurs and shows significant chattering with lower amplitude in the BSTA compared to the STA.

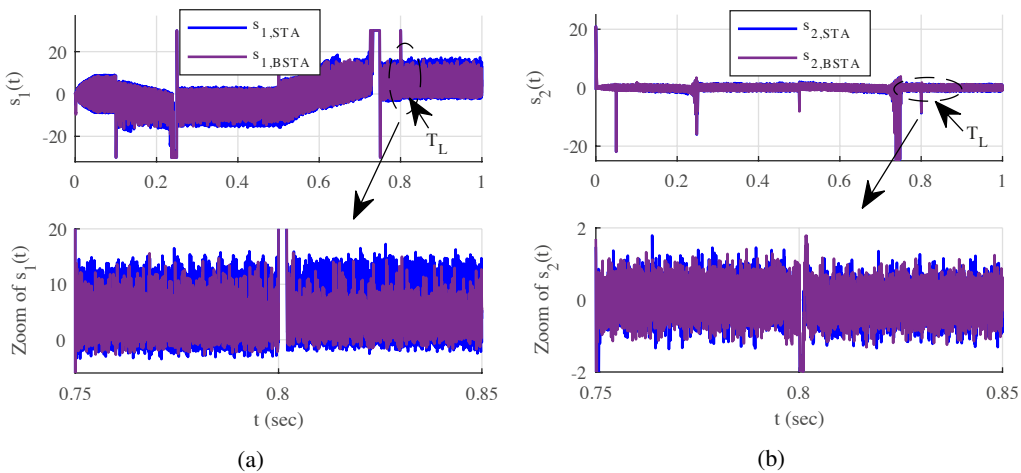


Fig. 7. Sliding surfaces outputs under speed variations: surfaces for speed (a); surfaces for flux (b)

5.2. Parameter uncertainties

The steady-state performance has a close connection with the rotor time constant, i.e. with the rotor resistance. In practice, the thermal effect can change this resistance value, accordingly, affect control stability, also, the mathematical model of the SOSM observer no longer matches the real machine. Therefore, in this last subsection, the robustness and effectiveness of our algorithms are tested against parameter uncertainties.

Let's assume that the rotor resistance increases by 100% of the nominal rate, and at the same time we increase the inertia value by about 30% of the nominal one.

Figure 8 evidences the rotor speed response of the STA and BSTA under these variations. For both algorithms, the settling time and rise time are affected by these parameters' variation. Furthermore, the responses are very satisfactory and there is a good torque rejection of $t = 0.5$ s.

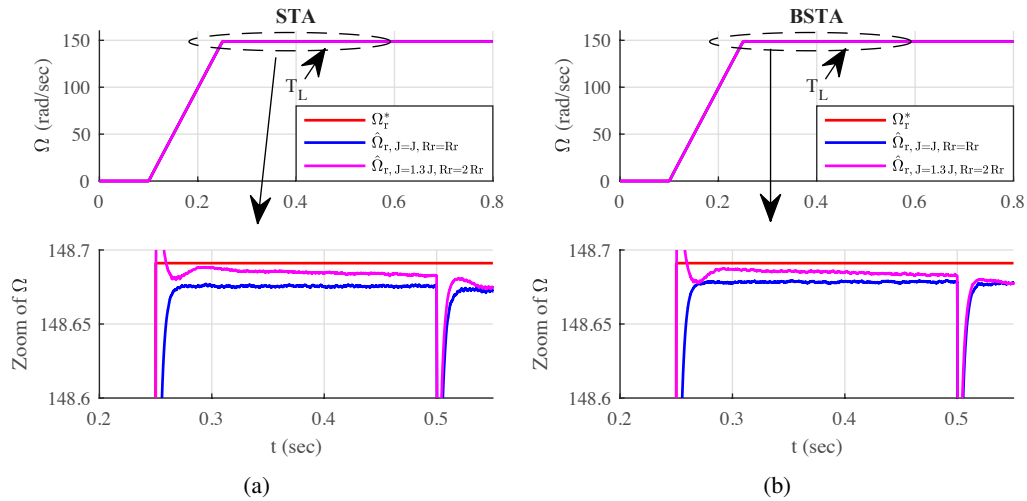


Fig. 8. Dynamic responses of rotor speed under variations of R_r and J ($+100\%R_r$, $+30\%J$)

Meanwhile, the fluxes estimated in Fig. 9 are affected by these variations, as they experience some errors at a transitory time, the zoom shows this fact. At a steady state, the decoupling control

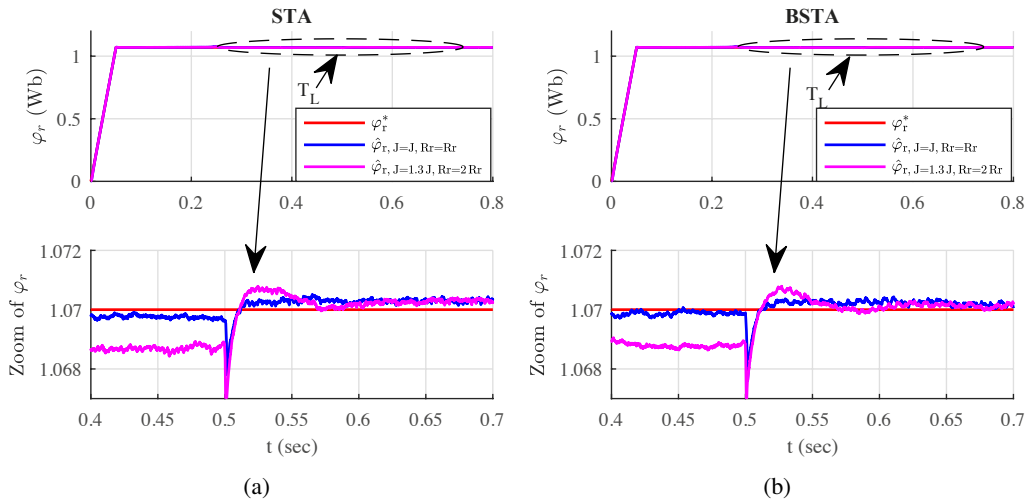


Fig. 9. Estimation of rotor flux during parameter variations

is ensured for the STA and BSTA, one can see that the fluxes estimated are not affected by the application of a load torque of $t = 0.5$ s.

Similarly, at the transitory time, the sliding surfaces are affected under parameter changes. At this time, the quasi-barrier function gains increase to counteract this perturbation. After a short time, the errors are eliminated in the STA and BSTA controllers and the surfaces converge towards zero with some chattering effects.

Generally, the simulation has indicated that the BSTA technique provides higher accuracy, lower chattering effect, and better robustness compared with the STA, and the SOSM observer offers accurate estimation. However, these results also need experimental verification.

6. Conclusions

In this paper, two robust SOSM algorithms have been applied to an induction motor. The super twisting algorithm is first applied to ensure finite-time convergence of the sliding surface outputs towards the origin, then, this algorithm is combined with quasi barrier function methodology to achieve better performance of the IM and to reduce high-frequency chattering, because the QBF methodology allows one to adapt the STA gains with sliding outputs, i.e. leads to variable gains according to perturbations in the system.

Moreover, to reduce the control system cost, the controlled output variables are estimated by the SOSM observer, which has proven its robustness against uncertainties. Additionally, the stability analysis has been presented using the Lyapunov theory.

Finally, a comparative study and a robustness assessment for both algorithms under different operating conditions have been carried out in MATLAB. The obtained results demonstrate the superiority of the BSTA technique over the STA in terms of the chattering reduction.

During the results obtained, both control techniques were not affected by the neglect of equivalent control, but the gains of control must be increased to get fast convergence. For the BSTA, there is possibility to adapt a barrier function boundary according to each operation condition. Such adaptation would be appropriate to improve the closed-loop dynamic and chattering alleviation.

References

- [1] Senthilnathan N., *Comparative analysis of line-start permanent magnet synchronous motor and squirrel cage induction motor under customary power quality indices*, Electrical Engineering, vol. 102, no. 3, pp. 1339–1349 (2020), DOI: [10.1007/s00202-020-00955-2](https://doi.org/10.1007/s00202-020-00955-2).
- [2] Morfin O.A., Miranda U., Valenzuela R.R., Valenzuela F.A., Tellez F.O., Acosta J.C., *State-feedback linearization using a robust differentiator combined with SOSM super-twisting for controlling the induction motor velocity*, 2018 IEEE International Autumn Meeting on Power, Electronics and Computing (ROPEC), Ixtapa, México, pp. 1–6 (2018), DOI: [10.1109/ROPEC.2018.8661477](https://doi.org/10.1109/ROPEC.2018.8661477).
- [3] Acikgoz H., *Real-time adaptive speed control of vector-controlled induction motor drive based on online-trained Type-2 Fuzzy Neural Network Controller*, International Transactions on Electrical Energy Systems (2021), DOI: [10.1002/2050-7038.12678](https://doi.org/10.1002/2050-7038.12678).

- [4] Chen C., Wu H., Lin Y., *Stator flux oriented multiple sliding-mode speed control design of induction motor drives*, Advances in Mechanical Engineering, vol. 13, no. 5, pp. 1–10 (2021), DOI: [10.1177/168781402111021734](https://doi.org/10.1177/168781402111021734).
- [5] Steinberger M., Horn M., Fridman L., *Variable-Structure Systems and Sliding-Mode Control: From Theory to Practice*, Springer International Publishing (2020).
- [6] Bartolini G., Levant A., Pisano A., Usai E., *Adaptive second-order sliding mode control with uncertainty compensation*, International journal of Control, vol. 89, no. 9 (2016), DOI: [10.1080/00207179.2016.1142616](https://doi.org/10.1080/00207179.2016.1142616).
- [7] Siddique N., Rehman F.U., *Hybrid synchronization and parameter estimation of a complex chaotic network of permanent magnet synchronous motors using adaptive integral sliding mode control*, Archives of Electrical Engineering, pp. 137056–137056 (2021), DOI: [10.24425/bpasts.2021.137056](https://doi.org/10.24425/bpasts.2021.137056).
- [8] Quintero-Manriquez E., Sánchez E., Felix R., *Induction motor torque control via discrete-time sliding mode*, World Autom. Congr., WAC, pp. 1–5 (2016), DOI: [10.1109/WAC.2016.7582984](https://doi.org/10.1109/WAC.2016.7582984).
- [9] Martínez-Fuentes C.A., Ventura U.P., Fridman L., *Chattering analysis of Lipschitz continuous sliding-mode controllers*, ArXiv200400819 Cs Eess (2020).
- [10] Utkin V., Poznyak A., Orlov Y.V., Polyakov A., *Chattering Problem in Road Map for Sliding Mode Control Design*, Springer International Publishing, pp. 73–82 (2020), DOI: [10.1007/978-3-030-41709-3](https://doi.org/10.1007/978-3-030-41709-3).
- [11] Chaabane H., Djalal Eddine K., Salim C., *Sensorless back stepping control using a Luenberger observer for double-star induction motor*, Archives of Electrical Engineering, vol. 69, no. 1, (2020), DOI: [10.24425/ae.2020.131761](https://doi.org/10.24425/ae.2020.131761).
- [12] Swikir A., Utkin V., *Chattering analysis of conventional and super twisting sliding mode control algorithm*, in 2016 14th International Workshop on Variable Structure Systems (VSS), pp. 98–102 (2016), DOI: [10.1109/VSS.2016.7506898](https://doi.org/10.1109/VSS.2016.7506898).
- [13] Utkin V., Hoon Lee, *Chattering Problem in Sliding Mode Control Systems*, in International Workshop on Variable Structure Systems (VSS'06), Alghero, Italy, pp. 346–350 (2006), DOI: [10.1109/VSS.2006.1644542](https://doi.org/10.1109/VSS.2006.1644542).
- [14] Sun X., Cao J., Lei G., Zhu J., *A Composite Sliding Mode Control for SPMSM Drives Based on a New Hybrid Reaching Law With Disturbance Compensation*, IEEE Transactions on Transportation Electrification, vol. 7, no. 3, pp. 1427–1436 (2021), DOI: [10.1109/TTE.2021.3052986](https://doi.org/10.1109/TTE.2021.3052986).
- [15] Jin Z., Sun X., Lei G., Zhu J., *Sliding Mode Direct Torque Control of SPMSMs Based on a Hybrid Wolf Optimization Algorithm*, IEEE Transactions on Industrial Electronics (2021), DOI: [10.1109/TIE.2021.3080220](https://doi.org/10.1109/TIE.2021.3080220).
- [16] Pérez-Ventura U., Fridman L., *Design of super-twisting control gains: A describing function based methodology*, Automatica, vol. 99, pp. 175–180 (2019), DOI: [10.1016/j.automatica.2018.10.023](https://doi.org/10.1016/j.automatica.2018.10.023).
- [17] Lascu C., Argeseanu A., Blaabjerg F., *Super twisting Sliding-Mode Direct Torque and Flux Control of Induction Machine Drives*, IEEE Transactions on Power Electronics, vol. 35, no. 5, pp. 5057–5065 (2020), DOI: [10.1109/TPEL.2019.2944124](https://doi.org/10.1109/TPEL.2019.2944124).
- [18] Krim S., Gdaim S., Mimouni M.F., *Robust Direct Torque Control with Super-Twisting Sliding Mode Control for an Induction Motor Drive*, Complexity (2019), DOI: [10.1155/2019/7274353](https://doi.org/10.1155/2019/7274353).
- [19] Zhang L., Laghrouche S., Harmouche M., Cirrincione M., *Super twisting control of linear induction motor considering end effects with unknown load torque*, in 2017 American Control Conference (ACC), Seattle, USA, pp. 911–916 (2017), DOI: [10.23919/ACC.2017.7963069](https://doi.org/10.23919/ACC.2017.7963069).
- [20] Utkin V.I., Poznyak A.S., Ordaz P., *Adaptive super-twist control with minimal chattering effect*, in 2011 50th IEEE Conference on Decision and Control and European Control Conference, Orlando, FL, USA, pp. 7009–7014 (2011), DOI: [10.1109/CDC.2011.6160720](https://doi.org/10.1109/CDC.2011.6160720).

- [21] Gonzalez T., Moreno J.A., Fridman L., *Variable Gain Super-Twisting Sliding Mode Control*, IEEE Transactions on Automatic Control, vol. 57, no. 8, pp. 2100–2105 (2012), DOI: [10.1109/TAC.2011.2179878](https://doi.org/10.1109/TAC.2011.2179878).
- [22] Obeid H., Laghrouche S., Fridman L., Chitour Y., Harmouche M., *Barrier Function-Based Adaptive Super-Twisting Controller*, IEEE Transaction on Automatic Control, vol. 65, no. 11, pp. 4928–4933 (2020), DOI: [10.1109/TAC.2020.2974390](https://doi.org/10.1109/TAC.2020.2974390).
- [23] Obeid H., Fridman L.M., Laghrouche S., Harmouche M., *Barrier function-based adaptive sliding mode control*, Automatica, vol. 93, pp. 540–544 (2018), DOI: [10.1016/j.automatica.2018.03.078](https://doi.org/10.1016/j.automatica.2018.03.078).
- [24] Obeid H., Fridman L., Laghrouche S., Harmouche M., *Barrier Function-Based Adaptive Twisting Controller*, in 2018 15th International Workshop on Variable Structure Systems (VSS), Graz, Austria, pp. 198–202 (2018), DOI: [10.1109/VSS.2018.8460272](https://doi.org/10.1109/VSS.2018.8460272).
- [25] Svečko R., Gleich D., Sarjaš A., *The Effective Chattering Suppression Technique with Adaptive Super-Twisted Sliding Mode Controller Based on the Quasi-Barrier Function; An Experimentation Setup*, Applied Sciences, vol. 10, no. 2 (2020), DOI: [10.3390/app10020595](https://doi.org/10.3390/app10020595).
- [26] Horch M., Boumédiène A., Baghli L., *Sensorless high-order sliding modes vector control for induction motor drive with a new adaptive speed observer using super-twisting strategy*, Int. J. Computer Application in Technology, vol. 60, no. 2, pp. 144–153 (2019), DOI: [10.1504/IJCAT.2019.100131](https://doi.org/10.1504/IJCAT.2019.100131).
- [27] Morfin O.A., Valenzuela F.A., Betancour R.R., Castañeda C.E, Ruíz-Cruz R., Valderrabano-Gonzalez A., *Real-Time SOSM Super-Twisting Combined with Block Control for Regulating Induction Motor Velocity*, IEEE Access, vol. 6, pp. 25898–25907 (2018), DOI: [10.1109/ACCESS.2018.2812187](https://doi.org/10.1109/ACCESS.2018.2812187).
- [28] Listwan J., *Application of Super-Twisting Sliding Mode Controllers in Direct Field-Oriented Control System of Six-Phase Induction Motor: Experimental Studies*, Power Electronics and Drives, vol. 3, no. 1, pp. 23–34 (2018), DOI: [10.2478/pead-2018-0013](https://doi.org/10.2478/pead-2018-0013).
- [29] Lascu C., Blaabjerg F., *Super-twisting sliding mode direct torque control of induction machine drives*, in 2014 IEEE Energy Conversion Congress and Exposition (ECCE), pp. 5116–5122 (2014), DOI: [10.1109/ECCE.2014.6954103](https://doi.org/10.1109/ECCE.2014.6954103).
- [30] Rao S., Buss M., Utkin V., *Simultaneous State and Parameter Estimation in Induction Motors Using First- and Second-Order Sliding Modes*, IEEE Transactions on Transportation Electrification, vol. 56, no. 9, pp. 3369–3376 (2009), DOI: [10.1109/TIE.2009.2022071](https://doi.org/10.1109/TIE.2009.2022071).
- [31] Aurora C., Ferrara A., *A sliding mode observer for sensorless induction motor speed regulation*, International Journal of Systems Science, vol. 38, no. 11, pp. 913–929 (2007), DOI: [10.1080/00207720701620043](https://doi.org/10.1080/00207720701620043).
- [32] Sun X., Cao J., Lei G., Guo Y., Zhu J., *A Robust Deadbeat Predictive Controller With Delay Compensation Based on Composite Sliding-Mode Observer for PMSMs*, IEEE Transactions on Power Electronics, vol. 36, no. 9, pp. 10742–10752 (2021), DOI: [10.1109/TPEL.2021.3063226](https://doi.org/10.1109/TPEL.2021.3063226).
- [33] Riaz Ahamed S., Chandra Sekhar J.N., Dinakara Prasad Reddy P., *Speed Control of Induction Motor by Using Intelligence Techniques*, Journal of Engineering Research and Applications, vol. 5, no. 1, pp. 130–135(2015).
- [34] Dávila A., Moreno J.A., Fridman L., *Optimal Lyapunov function selection for reaching time estimation of Super Twisting algorithm*, in Proceedings of the 48th IEEE Conference on Decision and Control (CDC) held jointly with 2009 28th Chinese Control Conference, Shanghai, China, pp. 8405–8410 (2009), DOI: [10.1109/CDC.2009.5400466](https://doi.org/10.1109/CDC.2009.5400466).
- [35] Tee K.P., Ge S.S., Tay E.H., *Barrier Lyapunov Functions for the control of output-constrained nonlinear systems*, Automatica, pp. 918–927 (2009), DOI: [10.1016/j.automatica.2008.11.017](https://doi.org/10.1016/j.automatica.2008.11.017).

- [36] Obeid H., Fridman L., Laghrouche S., Harmouche M., Golkani M.A., *Adaptation of Levant's differentiator based on barrier function*, International Journal of Control, vol. 91, no. 9, pp. 2019–2027(2018), DOI: [10.1080/00207179.2017.1406149](https://doi.org/10.1080/00207179.2017.1406149).
- [37] Rolek J., Utrata G., Kaplon A., *Robust speed estimation of an induction motor under the conditions of rotor time constant variability due to the rotor deep-bar effect*, Archives of Electrical Engineering, vol. 69, no. 2, pp. 319–333 (2020), DOI: [10.24425/ae.2020.133028](https://doi.org/10.24425/ae.2020.133028).
- [38] Kiani B., Mozafari B., Soleymani S., Mohammad Nezhad Shourkaei H., *Predictive torque control of induction motor drive with reduction of torque and flux ripple*, Archives of Electrical Engineering (2021), DOI: [10.24425/bpasts.2021.137727](https://doi.org/10.24425/bpasts.2021.137727).